

***Supporting Information: Flow properties reveal the  
particle-to-polymer transition of ultra-low crosslinked microgels***

A. Scotti,<sup>1,\*</sup> M. Brugnoli,<sup>1</sup> C. G. Lopez,<sup>1</sup> S. Bochenek,<sup>1</sup> J. Crassous,<sup>1</sup> and W. Richtering<sup>1,†</sup>

<sup>1</sup>*Institute of Physical Chemistry, RWTH Aachen University, 52056 Aachen, Germany*

(Dated: November 27, 2019)

---

\* andrea.scotti@rwth-aachen.de

† richtering@rwth-aachen.de

## I. DYNAMIC LIGHT SCATTERING

The size distributions of the microgel solutions have been obtained from Contin analysis [1, 2] of the autocorrelation functions measured with multi-angle dynamic light scattering. The analyses have been performed with a customized Contin algorithm that uses the so-called L-curve criteria [3] to choose the regularizer parameter [4]. The value of this regularizer parameter strongly affects the width of the obtained size distribution [1, 2, 4]. Therefore, our algorithm aims to find the best value of the regularizer parameter for the inversion problem, i.e. the value of the regularizer parameter that leads to a solution that does neither penalized the goodness of the fit nor the smoothness of the solution.

Briefly, for every scattering angle, the Contin analysis is performed for 15 different values of the regularizer parameter between 0.01 and 10. The goodness of the fit, i.e. the residual norm, and the smoothness of the obtained size distribution, i.e. the squared value of the second derivative of the size distribution, are then computed for each analysis. Then, the values of the second derivative of the size distribution are plotted versus the residual norm. In this representation, the data follow the so-called L-shaped course. This is the typical behavior of the data during an optimization process. It has been shown that the best analysis is performed choosing the the value of the regularizer parameter corresponding to the corner of the curve [3–6].

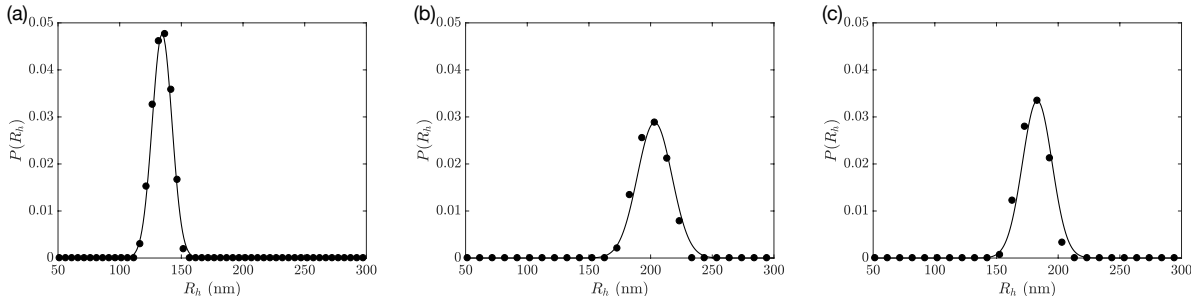


FIG. S1. Size distributions of ultra-low crosslinked microgels (a), 1 mol% crosslinked (b) and 10 mol% crosslinked microgels as obtained from a customized Contin algorithm [4]. All the measurements have been performed at  $20.0 \pm 0.01$  °C.

Once we have identified the best value of the regularizer parameter for each angle, the size distributions are obtained. Finally, the size distributions are fitted with a Gaussian as shown in figure S1. The width of the resulting fit is used as value for the polydispersity,

$p$ . The values reported in the last column of Tab. S1 are the average over the values of  $p$  obtained for the different scattering angles. The errors are the standard deviations of these values.

## II. SMALL-ANGLE SCATTERING

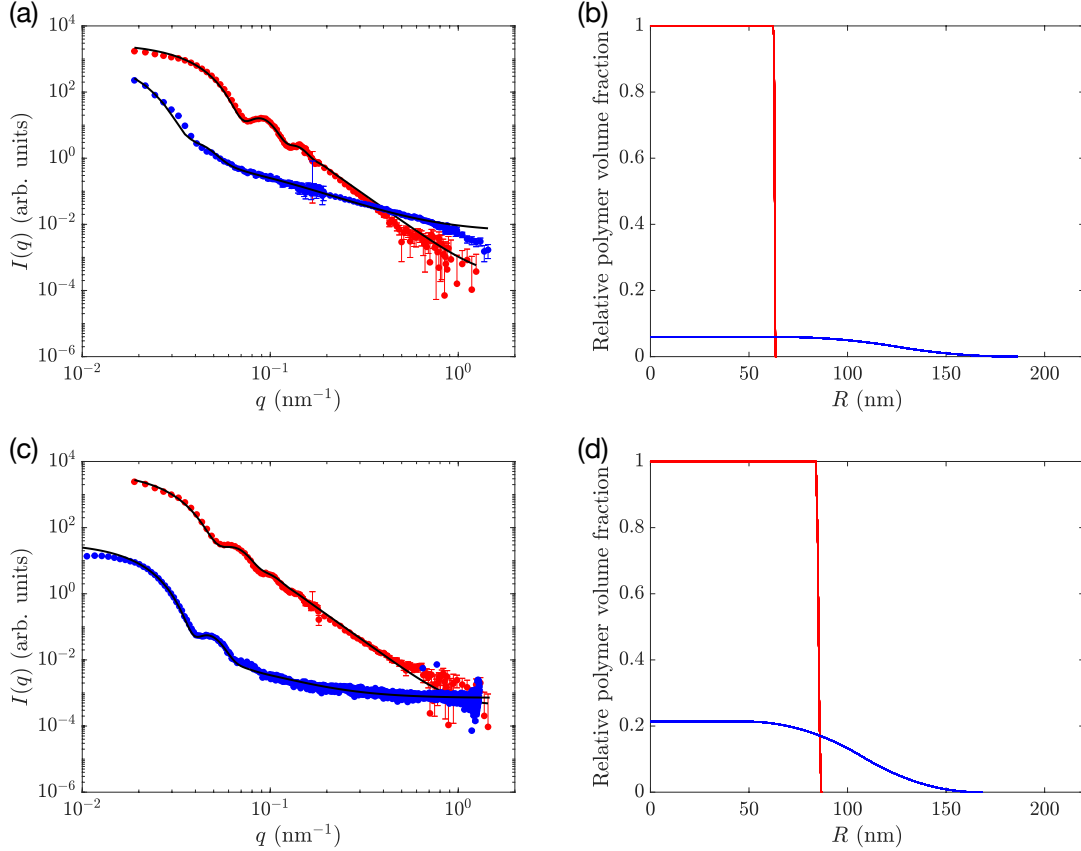


FIG. S2. Small-angle neutron or X-ray scattered intensity,  $I(q)$ , versus scattering vector,  $q$ , for (a) regular 1 mol% crosslinked microgels (SANS) and (c) 10 mol% crosslinked microgel (SANS red, SAXS blue). Red dots:  $T = 40$  °C. Blue dots:  $T = 20$  °C. Solid lines fit of the data with the fuzzy-sphere model [7]. (b) and (d) relative polymer radial distribution within the microgel for regular 1 mol% crosslinked microgels and 10 mol% crosslinked microgel, respectively. Red lines:  $T = 40$  °C. Blue lines:  $T = 20$  °C.

The small-angle neutron scattering (SANS) measurements were done using the KWS-2 instrument operated by JCNS at the Heinz Maier-Leibnitz Zentrum (MLZ, Garching, Germany). Three configurations have been used to cover the  $q$ -range of interest: sample

detector distance,  $d_{\text{SD}} = 20$  m with neutron wavelength  $\lambda = 1$  nm;  $d_{\text{SD}} = 8$  m with  $\lambda = 0.5$  nm; and  $d_{\text{SD}} = 2$  m with  $\lambda = 0.5$  nm. The  $\lambda$ -resolution was 10 % due to the velocity selector. The instrument mounts a  $^3\text{He}$  detector with a pixel size  $< 8$  mm.

cSAXS instrument at the Swiss Light Source, Paul Scherrer Institut (Villigen, Switzerland) was used to collect the small-angle X-ray scattering (SAXS) data. X-rays with a wavelength  $\lambda = 0.143$  nm and an error of 0.02 % over  $\lambda$  resolution were used. The  $q$ -range of interest was covered with a sample detector distance of 7.12 m. The collimated beam had an area of about  $200 \mu\text{m} \times 200 \mu\text{m}$ . The instrument had a 2D detector with a pixel size of  $172 \mu\text{m}$  and  $1475 \times 1679$  pixels.

Fig. S2(a) and S2(c) illustrates the scattered intensities,  $I(q)$ , of 1 mol% and 10 mol% crosslinked microgels in the swollen (blue) and deswollen (red) state, respectively, with the fits with the fuzzy-sphere model (solid lines) [7]. Figs. S2(b) and S2(d) show the corresponding radial density distributions. At 40 °C, the microgels are collapsed and reveal a box-like profile (red lines). At 20 °C, the microgels are swollen by the solvent and possess the typical core-fuzzy-corona structure (blue lines) [7].

### III. VISCOSIMETRY

TABLE S1. Sample names and labels of the synthesized batches with corresponding conversion constants,  $k$ , from viscosity measurements (third column), hydrodynamic radii and size polydispersities for the samples as obtained from DLS data (forth and fifth columns) at 20 °C.

Sample	Label	Viscosimetry	DLS	
		$k$	$R_h$ (nm)	$p$ (%)
ULC	<i>MB-ULC-140-PNIPAM</i>	$44.7 \pm 0.1$	$134 \pm 1$	$10 \pm 1$
regular 1 mol%	<i>MB-MK-pNIPAM-1APMH-1BIS</i>	$36.0 \pm 0.6$	$208 \pm 1$	$9.5 \pm 0.3$
regular 10 mol%	<i>MB-MK-pNIPAM-1APMH-10BIS</i>	$9.9 \pm 0.1$	$184.8 \pm 0.9$	$9 \pm 1$

The relative viscosity,  $\eta_r$ , versus the mass fraction,  $c$ , of the ultra-low crosslinked microgels, 1 mol% and 10 mol% regularly crosslinked microgels are plotted in Figs. S3(a), S3(b) and S3(c), respectively. The solid lines are the fits of the data with the Einstein-Batchelor

equation [8], Eq. 3 in the main text where  $\phi$  is substituted with  $kc$ . The values of the conversion constants as obtained from the data fit,  $k$ , are summarized in the third column of Tab. S1.  $k$  values are used to convert mass concentrations in generalized volume fractions:  $\zeta = kc$ .

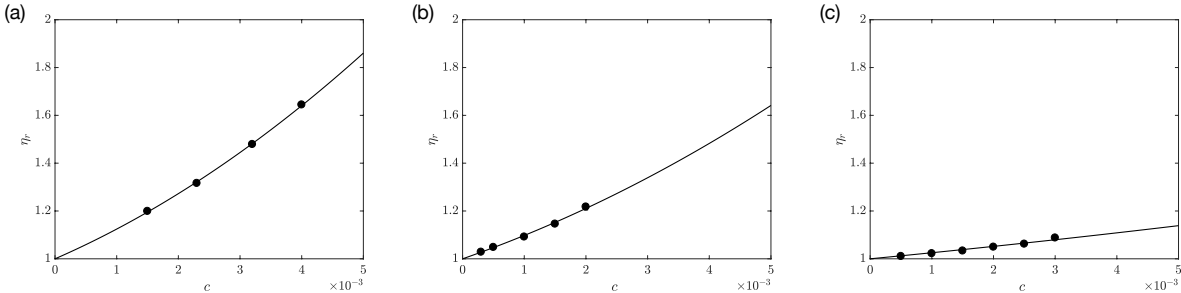


FIG. S3. Relative viscosity,  $\eta_r$ , versus mass fraction,  $c$ , for ultra-low crosslinked microgels (a), 1 mol% crosslinked microgels (b) and 10 mol% crosslinked microgels (c). Solid lines: fits obtained from Eq. 3 in the main text.

#### IV. VALIDATION OF THE CONVERSION CONSTANT OBTAINED FROM VISCOSITY MEASUREMENTS

The generalized volume fraction  $\zeta$  can be written as  $NV_{sw}/V_{tot}$  where  $N$  is the number of microgels in solution,  $V_{sw}$  and  $V_{tot}$  are the volume of the swollen microgel in dilute condition and the total volume of the solution, respectively. The latter can be computed from the solvent density.

$V_{sw}$  is calculated from the hydrodynamic radius of the microgels in the swollen state as obtained from DLS:  $V_{sw} = \frac{4}{3}\pi R_{h,T=20^\circ\text{C}}^3$ .

$N$  can be determined once the molecular weight of the microgel,  $M_w$ , is known. A direct method to do this is to use static light scattering and the so called Zimm-plot [9, 10]. The results of this method are shown in Fig. S4 and allow to estimate the molecular weight of the ultra-low crosslinked microgels:  $M_w^{SLS} = (1.26 \pm 0.02) \cdot 10^8$  g/mol. Since we know the mass of polymer used to prepare the solutions,  $m_{pNIPAM}$ , using  $M_w^{SLS}$  and  $N_A$ , the Avogadro constant,  $N$  is computed:  $N = (m_{pNIPAM}N_A)/M_w$ . In this way we are able to compute  $\zeta_{SLS} = NV_{sw}/V_{tot}$ .

In literature, the most common method to access the generalized volume fraction of

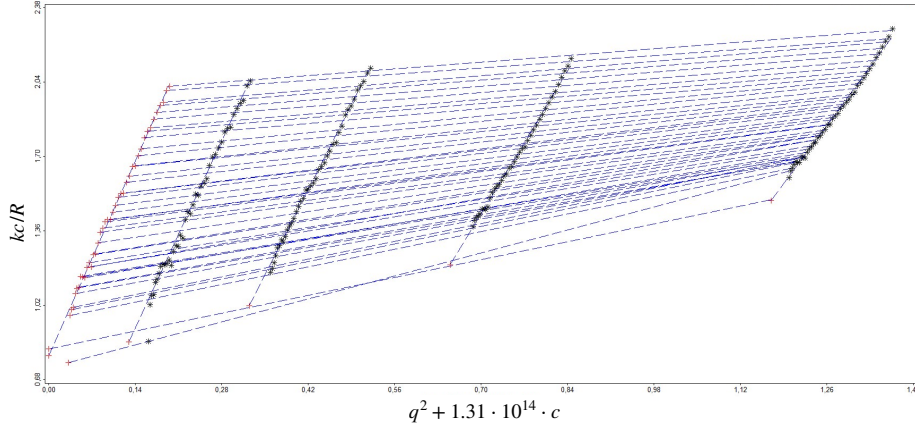


FIG. S4. Zimm plot for the ultra-low crosslinked microgels.

microgels in solutions consists in measuring the viscosity of dilute solutions of microgels. Then the data  $\eta_r$  versus  $c$  are fitted with the Einstein-Batchelor equation (Eq. 3 in the main text with  $\phi = \zeta = kc$ , Fig. S3). In this way, a conversion constant between mass fraction and generalized volume fraction,  $k$ , is obtained and used to compute the generalized volume fraction of the samples,  $\zeta_{visc} = kc$ .

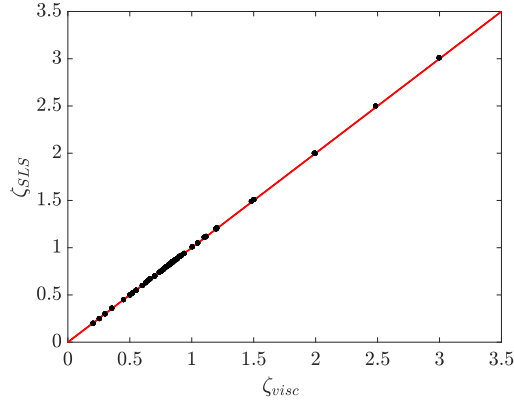


FIG. S5. Generalized volume fraction calculated with the conversion constant obtained by fitting viscosity data in the highly dilute regime with the Einstein-Batchelor Equation,  $\zeta_{visc}$  versus generalized volume fraction obtained using the molecular weight as measured by static light scattering,  $\zeta_{SLS}$ . The red line has slope 1 and intercepts the origin of the axes.

In Fig. S5,  $\zeta_{visc}$  is plotted versus  $\zeta_{SLS}$ . The data lie on the red solid line, which has a slope equal to 1 and intercept in the axes origin at  $\zeta_{SLS} = \zeta_{visc} = \zeta$ . The two methods lead

to the same value of  $\zeta$ . This justifies the use of the Einstein-Batchelor equation to describe the viscosity of the solutions in highly diluted regime and also the use of the conversion constant  $k$  to compute the generalized volume fraction starting from the mass concentration  $c$ .

## V. QUEMADA MODEL

Models developed to describe the increase of viscosity with suspension concentration for hard incompressible colloids have been often used to describe also the trend of the viscosity versus packing fraction of solutions of microgels. A typical example is the model proposed by Quemada [11] that has successfully been applied to describe the viscosity of microgel solutions [12]:

$$\eta_r = \left(1 - \frac{\zeta}{\zeta_{g,Q}}\right)^{-2} \Rightarrow \eta_r^{-0.5} = 1 - \frac{\zeta}{\zeta_{g,Q}}, \quad (\text{S1})$$

where  $\zeta_{g,Q}$  is the value of the glass transition. In Fig. S6, the inverse of the square root of the relative viscosity,  $\eta_r^{-0.5}$ , is plotted versus the generalized volume fraction,  $\zeta$ . The data are fitted with a linear regression according to Eq. S1.  $\zeta_{g,Q}$  is the intercept with the  $x$ -axis [12]. It is evident that the data of the ULC microgels are not described by this model. In contrast, the data for the 1 and 10 mol% crosslinked microgels follow Eq. S1 as expected.

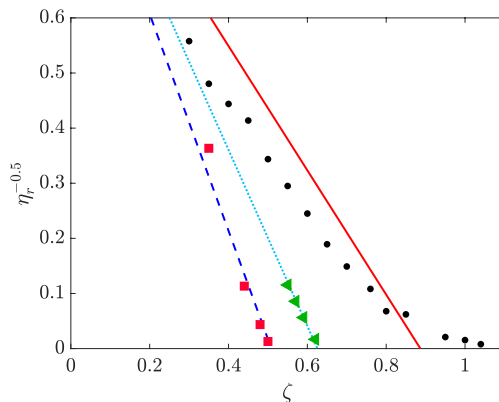


FIG. S6. Inverse of the square root of the relative viscosity,  $\eta_r^{-0.5}$ , versus generalized volume fraction,  $\zeta$ , for: ULC microgels (circles), 1 mol% crosslinked microgels (triangles), 10 mol% crosslinked microgels (squares). The solid lines represent linear fits of the data with Eq. S1.

## VI. PARAMETERS OF THE CROSS MODEL

The values of the fit parameters as obtained from Cross' equation, Eq. 1 in the main text, are reported in Fig. S7 as a function of  $\zeta$ .

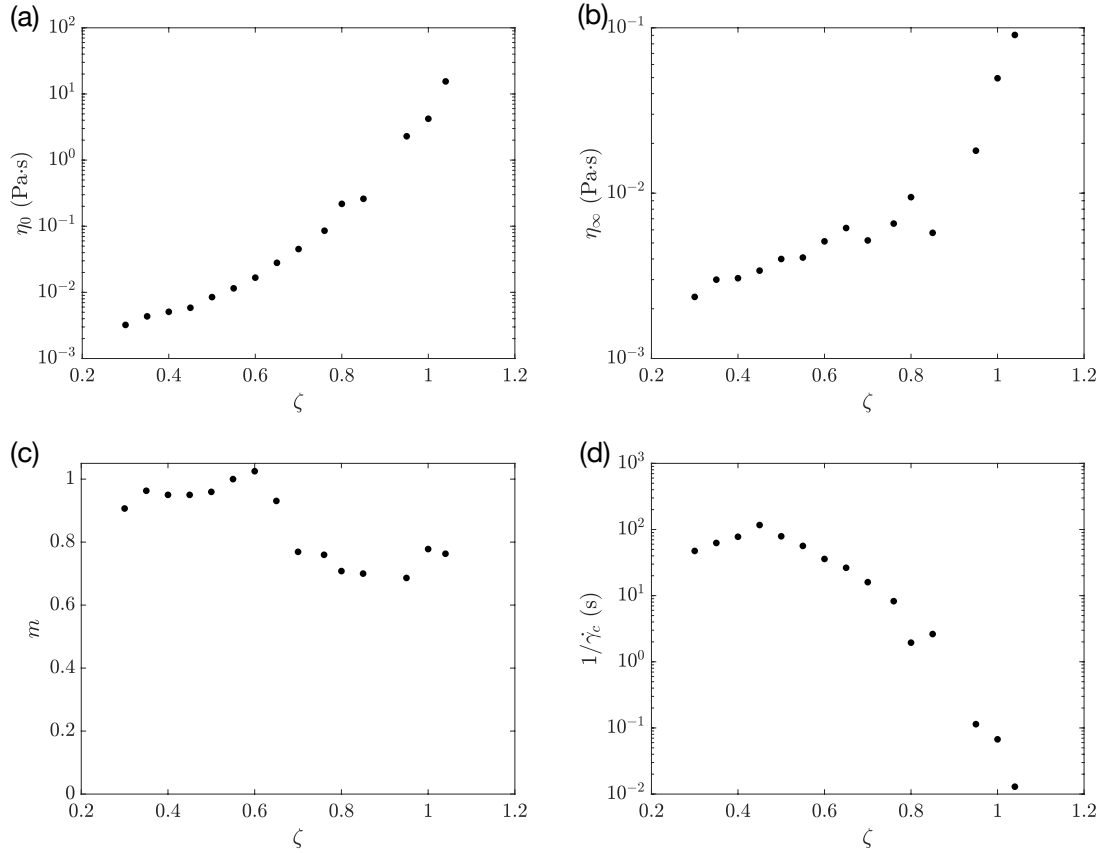


FIG. S7. Course of the values of the fit parameters as obtained from the Cross equation used to fit the viscosity of the suspensions of ULC microgels as a function of  $\zeta$ : (a)  $\eta_0$ ; (b)  $\eta_\infty$ ; (c)  $m$ ; (d)  $1/\dot{\gamma}_c$ .

## VII. RHEOLOGY

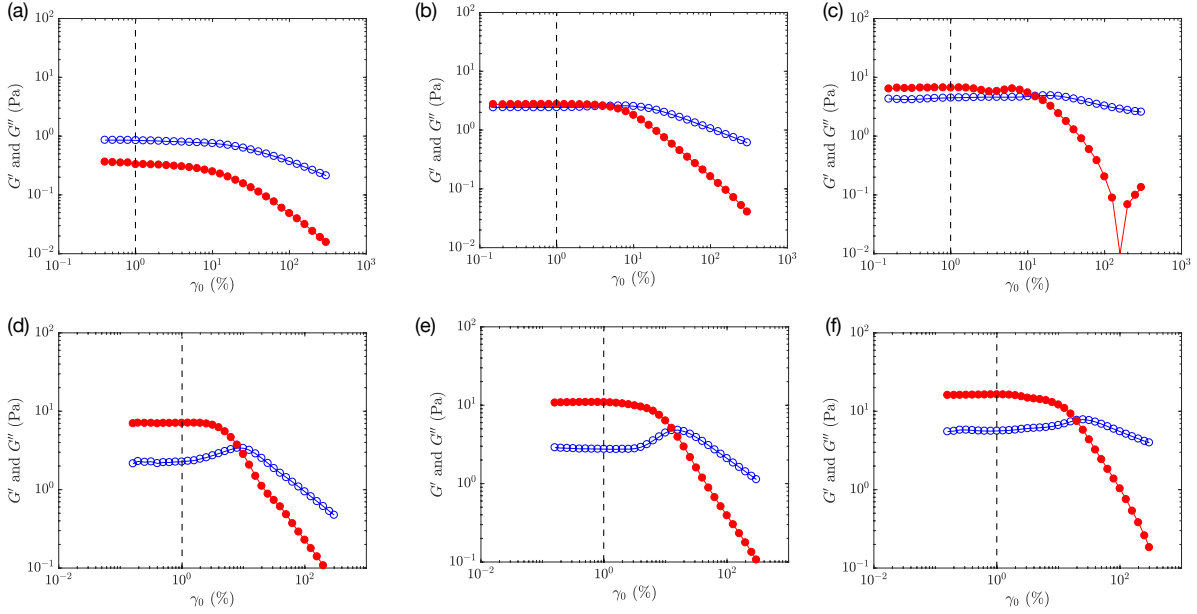


FIG. S8. Storage modulus (red full circles),  $G'$ , and loss modulus (empty blue circles),  $G''$ , versus  $\gamma_0$ , for ULC suspensions with:  $\zeta = 0.95 \pm 0.02$  and  $\omega = 0.1$  Hz (a);  $\zeta = 0.95 \pm 0.02$  and  $\omega = 1$  Hz (b);  $\zeta = 0.95 \pm 0.02$  and  $\omega = 10$  Hz (c);  $\zeta = 1.10 \pm 0.03$  and  $\omega = 0.1$  Hz (d);  $\zeta = 1.10 \pm 0.03$  and  $\omega = 1$  Hz (e);  $\zeta = 1.10 \pm 0.03$  and  $\omega = 10$  Hz (f). All measurements have been performed at  $(20.0 \pm 0.01)^\circ\text{C}$  and after rejuvenation process. Dashed lines correspond to  $\gamma_0 = 1\%$  of the gap.

Fig. S8 shows some examples of the storage and loss moduli as a function of  $\gamma_0$  for  $\omega = 0.1$  Hz (a) and (d),  $\omega = 1$  Hz (b) and (e), and  $\omega = 10$  Hz (c) and (f). The dashed lines mark the correspondence to  $\gamma_0 = 1\%$ . The suspensions are in the linear viscoelastic region for  $0.1 \text{ Hz} < \omega < 10 \text{ Hz}$  at  $\gamma_0 = 1\%$  of the gap.

Fig. S9 shows the results of oscillatory frequency sweep measurements for  $\omega$  between 0.1 and 10 Hz and  $\gamma = 1\%$  of the gap. In these experiments, the viscoelastic spectra of microgel suspensions are recorded. The panels refer to measurements of suspensions of ULC microgels (top line) and 1 mol% crosslinked microgels (bottom line) for increasing concentrations (from left to right). As shown in Fig. S8, for the values of  $\gamma_0$  and  $\omega$  used in these experiments, the suspensions are in the linear viscoelastic region.

As describe in the main manuscript, before every acquisition, the samples were shear-melted by applying a constant shear stress for 60 s. Therefore, we have performed acqui-

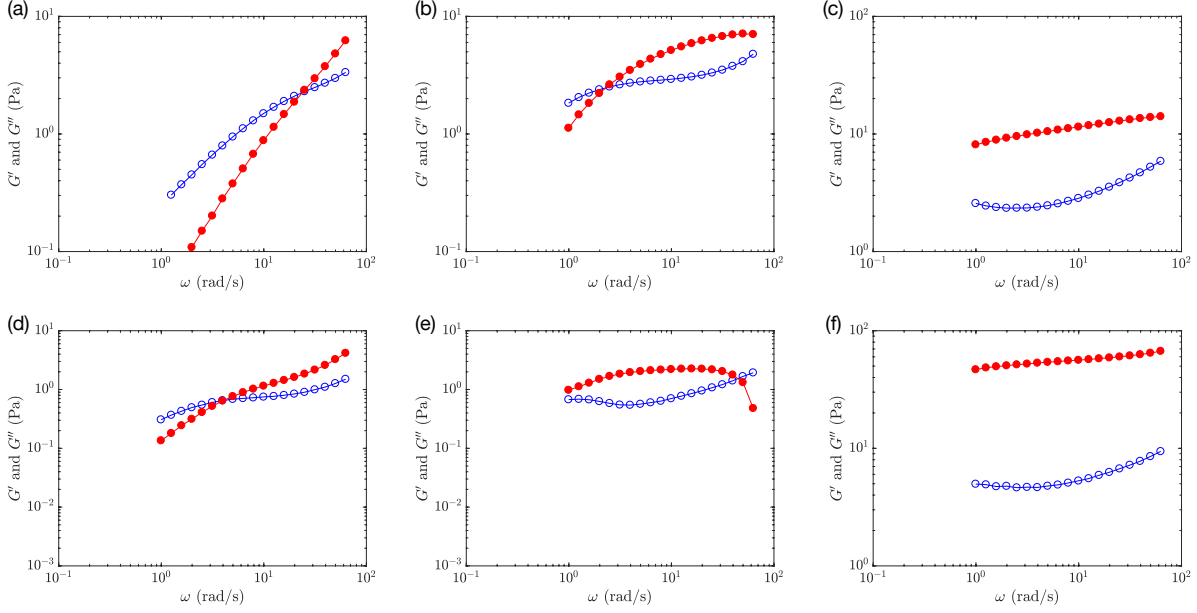


FIG. S9. Storage modulus (red full circles),  $G'$ , and loss modulus (empty blue circles),  $G''$ , versus the frequency,  $\omega$ , for ULC suspensions with  $\zeta = 0.85 \pm 0.01$  (a),  $\zeta = 1.00 \pm 0.03$  (b) and  $\zeta = 1.10 \pm 0.03$  (c) and for regular 1 mol% crosslinked microgels with  $\zeta = 0.59 \pm 0.01$  (d),  $\zeta = 0.62 \pm 0.01$  (e) and  $\zeta = 1.06 \pm 0.02$  (f). All measurements have been performed between  $\omega = 0.01$  Hz and  $\omega = 10$  Hz at  $\gamma_0 = 1$  % of the gap and after rejuvenation process.  $T$  was set to  $(20.0 \pm 0.01)$  °C.

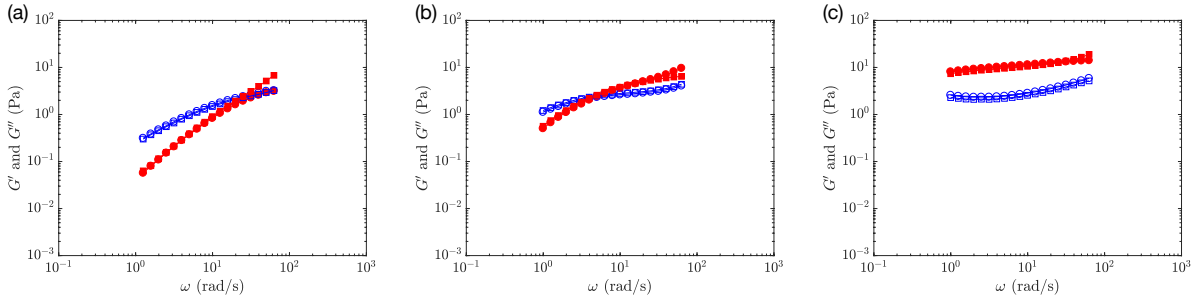


FIG. S10. Storage modulus (solid symbols),  $G'$ , and loss modulus (empty symbols),  $G''$ , versus the frequency,  $\omega$ , for ULC suspensions with  $\zeta = 0.85 \pm 0.01$  (a),  $\zeta = 0.95 \pm 0.02$  (b) and  $\zeta = 1.10 \pm 0.04$  (c). The measurements were performed 60 s (circles) and 7200 s (squares) after the shear-melting process (rejuvenation process). All measurements have been performed between  $\omega = 0.01$  Hz and  $\omega = 10$  Hz at  $\gamma_0 = 1$  % of the gap.  $T$  was set to  $(20.0 \pm 0.01)$  °C.

sitions waiting for different times after applying a constant shear stress for 60 s to verify whether the samples were ageing. Fig. S10 shows the results of frequency sweep mea-

measurements performed 60 and 7200 s after shear-melting the samples for 60 s. No signs of significant ageing are visible.

### VIII. VALIDITY OF THE LINEAR DEPENDENCE OF $G_p$ VERSUS $\zeta$

As discussed in the main text in section 3.3 it is crucial to understand in which concentration range  $G_p$  follows Eq. 6. In Fig. S11(a) we use Eq. 6 to fit the trend of  $G_p$  versus  $\zeta$  for high packing fractions. The concentration range at where the linear dependence holds is selected by choosing different intervals and performing the fit with Eq. 6. Then the “best” interval is chosen by comparing the  $\chi^2$  of the different fits and choosing the region where  $\chi^2$  is the smallest. The resulting intervals and best linear fits are shown in Fig. S11(a).

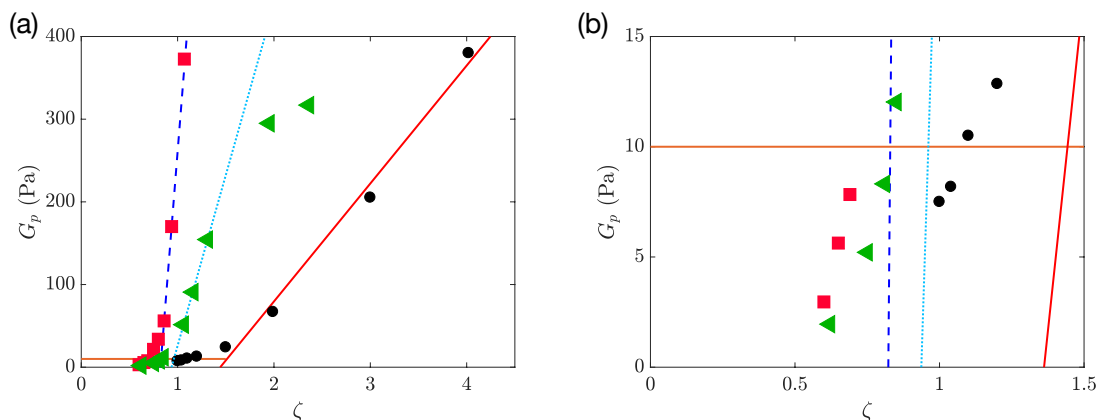


FIG. S11. (a)  $G_p$  versus  $\zeta$  for the 10 mol% (squares), 1 mol% (triangles) and ultra-low crosslinked (circles) microgels. The blue, light blue and red lines are linear fits of the data at high concentrations. The orange horizontal line is at approximately  $k_B T/R_h^3$ . (b) Magnification of the left graph to the low  $\zeta$ -regime.

However, as mentioned in the main text, at low concentrations the data cannot be considered as flat and, therefore, fitted to a constant value  $\approx k_B T/R_h^3$ . This is shown in Fig. S11(b).

---

[1] S. W. Provencher, Computer Physics Communications **27**, 213 (1982).

- [2] S. W. Provencher, *Computer Physics Communications* **27**, 229 (1982).
- [3] P. C. Hansen, *Numerical Algorithms* **6**, 1 (1994).
- [4] A. Scotti, W. Liu, J. S. Hyatt, E. S. Herman, H. S. Choi, J. Kim, L. A. Lyon, U. Gasser, and A. Fernandez-Nieves, *J. Chem. Phys.* **142**, 234905 (2015).
- [5] O. L. J. Virtanen, A. Mourran, P. T. Pinard, and W. Richtering, *Soft Matter* **12**, 3919 (2016).
- [6] P. C. Hansen, *Numerical Algorithms* **46**, 189 (2007).
- [7] M. Stieger, W. Richtering, J. S. Pedersen, and P. Lindner, *J. Chem. Phys.* **120**, 6197 (2004).
- [8] G. K. Batchelor, *J. Fluid Mech.* **83**, 97 (1977).
- [9] M. Brugnoli, A. C. Nickel, L. Kröger, A. Scotti, A. Pich, K. Leonhard, and W. Richtering, *Polym. Chem.* **10**, 2397 (2019).
- [10] S. Nöjd, C. Hirst, M. Obiols-Rabasa, J. Schmitt, A. Radulescu, P. S. Mohanty, and P. Schurtenberger, *Soft matter* **15**, 6369 (2019).
- [11] D. Quemada, *Rheologica Acta* **16**, 82 (1977).
- [12] F. M. Horn, W. Richtering, J. Bergenholtz, N. Willenbacher, and N. J. Wagner, *Journal of Colloid and Interface Science* **225**, 166 (2000).